APL Materials

Rhenium dinitride: Carrier transport in a novel transition metal dinitride layered crystal

Cite as: APL Mater. **7**, 101103 (2019); https://doi.org/10.1063/1.5118713
Submitted: 04 July 2019 . Accepted: 12 September 2019 . Published Online: 03 October 2019

Momoko Onodera, Fumio Kawamura, Nguyen Thanh Cuong, Kenji Watanabe, Rai Moriya, Satoru Masubuchi, Takashi Taniguchi, Susumu Okada, and Tomoki Machida

Rhenium dinitride: Carrier transport in a novel transition metal dinitride layered crystal

Cite as: APL Mater. 7, 101103 (2019); doi: 10.1063/1.5118713
Submitted: 4 July 2019 • Accepted: 12 September 2019 •
Published Online: 3 October 2019

Momoko Onodera,[1] Fumio Kawamura,[2] Nguyen Thanh Cuong,[3] Kenji Watanabe,[2] Rai Moriya,[1] Satoru Masubuchi,[1] Takashi Taniguchi,[2] Susumu Okada,[3] and Tomoki Machida[1,a)]

AFFILIATIONS

[1]Institute of Industrial Science, University of Tokyo, 4-6-1 Komaba, Meguro, Tokyo 153-8505, Japan
[2]National Institute for Materials Science, 1-1 Namiki, Tsukuba, Ibaraki 305-0044, Japan
[3]Graduate School of Pure and Applied Sciences, University of Tsukuba, 1-1-1 Tennodai, Tsukuba, Ibaraki 305-8571, Japan

[a)]**Author to whom correspondence should be addressed:** tmachida@iis.u-tokyo.ac.jp

ABSTRACT

Rhenium dinitride (ReN_2) is a newly synthesized layered transition metal dinitride. We present the first experimental investigation of the electrical transport properties of ReN_2 by exfoliating the ReN_2 crystal into thin films. The carrier transport measurements reveal that ReN_2 is a metal. Furthermore, ReN_2 exhibits suppression of resistance due to superconductivity at temperatures below 10 K. The critical magnetic fields differ significantly depending on the direction of the applied magnetic field, suggesting that ReN_2 is an anisotropic layered superconductor.

Various ultrahard crystals such as diamond[1,2] and cubic boron nitride (c-BN)[3,4] are grown using a high-pressure apparatus under high pressure and high temperature (HPHT) exceeding 4 GPa and 1300 °C, respectively, where the starting materials are melted at the high temperature and turned into a high density phase under the high pressure. In the HPHT method, the compressing process can also be utilized for the reduction of impurities. It has been demonstrated that the HPHT method is also valid for synthesis of high-quality layered materials such as hexagonal boron nitride (h-BN),[4] which is used in more than 200 research institutes worldwide as a high-quality insulating 2D material. The Ba–BN solvent used in the h-BN synthesis reduces O and C impurities under high pressure, improving the purity of the obtained crystals.

Rhenium dinitride (ReN_2) is another HPHT-synthesized material having a layered structure, which was synthesized in 2012 with the same apparatus used for HPHT h-BN.[5] ReN_2 was originally intended to be an ultrahard material comparable to diamond. However, ReN_2 did not have the expected mechanical strength. Instead, it had a layered shape, which was isostructural with conventional semiconductor transition metal dichalcogenides (TMDCs), such as MoS_2. Thus, ReN_2 should have been a fascinating material for the 2D research community because it was the first synthesized crystal of a layered transition metal dinitride (TMDN). Nevertheless, no experimental characterization has been made regarding the electronic properties of ReN_2. Even fundamental characteristics, such as whether ReN_2 is a metal, a semiconductor, or an insulator, are still unknown. The research status of ReN_2 is contrasted to that of rhenium dichalcogenides ReS_2 and $ReSe_2$, which are obtained using a modified Bridgman method[6] or chemical vapor deposition.[7,8] The rhenium dichalcogenides have been attracting attention owing to the distinctive properties originating from its uniquely distorted crystal structure[9] and the interesting properties[10–13] applied in the development of photodetectors and field-effect transistors (FETs).[14–16]

Subsequent to the synthesis of ReN_2, the second TMDN, MoN_2, was synthesized using a high-pressure route at a pressure of 3.5 GPa.[17] Furthermore, various types of TMDNs have been investigated using numerical simulation[18] to predict their band structures; in the form of one atomic layer, MoN_2, TcN_2, and ZrN_2 are expected to be metals, YN_2 a half-metal, and NbN_2 an insulator. YN_2 is of particular interest, being a promising material for spintronics.[19] Thus, TMDNs have the potential to be a fascinating material family, particularly in the research field of 2D materials. However, no experimental investigations have been performed that address the electronic properties of TMDNs. Thus, it is very important to reveal the nature

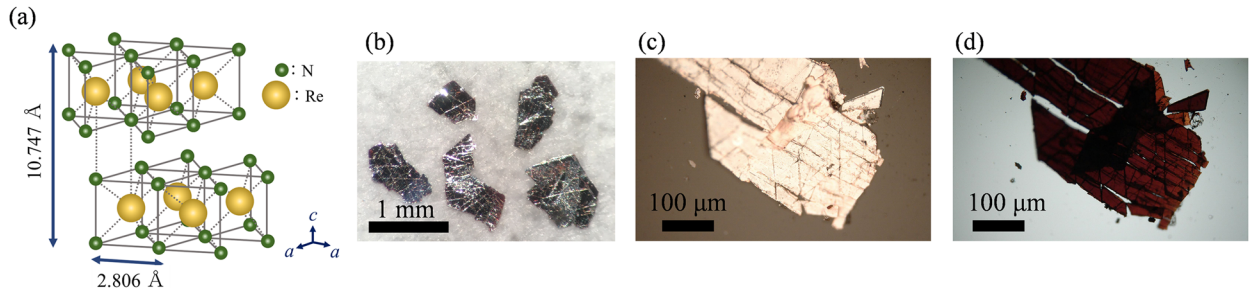

FIG. 1. (a) Schematic illustration of the ReN_2 crystal structure, which belongs to the space group $P6_3/mmc$. (b) Photographic image of ReN_2 crystals. Optical micrograph of the ReN_2 crystal with (c) reflected light and (d) transmitted light.

of TMDNs in order to expand a base layered/2D material for van der Waals heterostructures.

Figure 1(a) shows a schematic of the crystal structure of ReN_2; X-ray diffraction analysis[5] confirms that it belongs to the space group $P6_3/mmc$, which is isostructural with MoS_2. The ReN_2 crystal was synthesized using a metathesis reaction under high pressure (~7.7 GPa) and high temperature (~1873 K). The obtained crystal has a platelike shape, and its size is ~2 mm [Fig. 1(b)], slightly smaller than that of conventional layered crystals, such as bulk graphite, MoS_2, and h-BN. The most distinctive feature is its color; it shows metallic luster with reflected light [Fig. 1(c)], and it appears to be red with transmitted light under an optical microscope [Fig. 1(d)].

In bulk form, the ReN_2 crystal seems to be inappropriate for electrical measurements due to the many grain boundaries in the crystals. To obtain a flake without grain boundaries, we employed mechanical exfoliation of ReN_2 on a 290-nm-thick SiO_2/p-doped Si substrate using Scotch tape. We found some exfoliated flakes having sizes of 10–1000 μm^2. Figures 2(a) and 2(b) show an optical image and an atomic force microscopy (AFM) image of a ReN_2 flake. Figure 2(c) plots a height profile of the flake along the red line marked in Fig. 2(b), which shows a flat surface and a thickness of ~80 nm. We investigated other flakes, and the thinnest one was ~30 nm. We also obtained the Raman scattering spectra [Fig. 2(d)], the scanning transmission electron microscopy (STEM) image [Fig. 2(e)], and the energy-dispersive X-ray spectrometry (EDX) profile [Fig. 2(f)] of an ReN_2 flake, which is also used in transport measurements (Fig. S1). The STEM image and the EDX profile confirm a layered structure of ReN_2 with a period of ~1 nm, which is consistent with the c-axis length of ReN_2.

After finding relatively large flakes, electrodes were patterned on them using electron beam lithography followed by metal evaporation of Au 70 nm/Cr 10 nm. Figure 3(a) shows an optical micrograph of sample no. 1. The transport measurements were performed at T = 1.5–300 K in a variable-temperature insert (VTI) and at T = 0.06–4.2 K in a dilution refrigerator. A magnetic field was applied from a superconducting magnet. The sample was mounted on a rotating stage in the VTI and dilution refrigerator to tune the angle between the ReN_2 plane and the magnetic field. The four-terminal resistance R_{xx} was measured using a lock-in amplifier with an alternating current (I_{AC}) at a frequency of 18 Hz. The current–voltage (I-V) characteristics were measured by applying a direct current I_{DC} generated from a source meter. The differential resistance dV/dI was measured by applying I_{AC} imposed on I_{DC}.

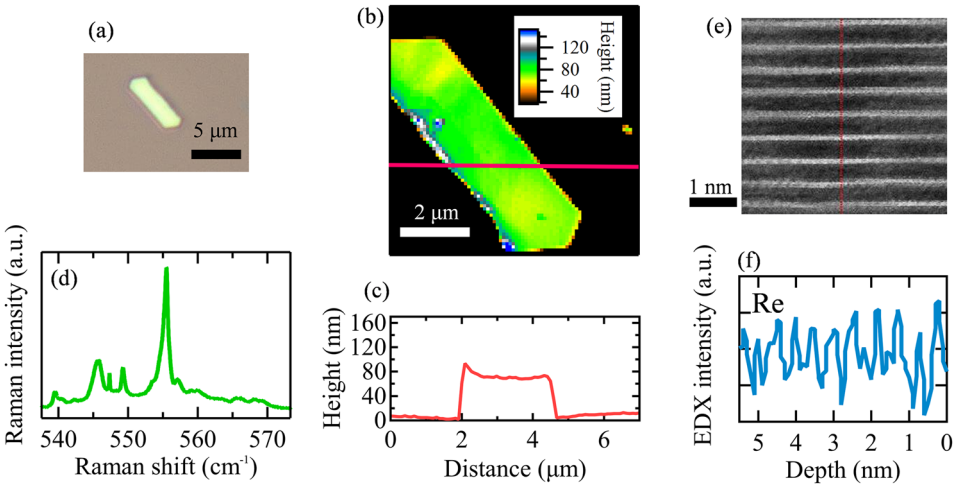

FIG. 2. (a) Optical image of an exfoliated ReN_2 flake on a SiO_2/Si substrate. (b) Atomic force microscopy topographic map of ReN_2 flake. (c) Height profile along the red line marked in (b). (d) Raman scattering spectrum of the exfoliated ReN_2 on a SiO_2/Si substrate. (e) Scanning transmission electron microscopy image of a cross section of the exfoliated ReN_2 on a SiO_2/Si substrate (sample no. 2). (f) Energy-dispersive X-ray spectrometry profile along the red line in (e).

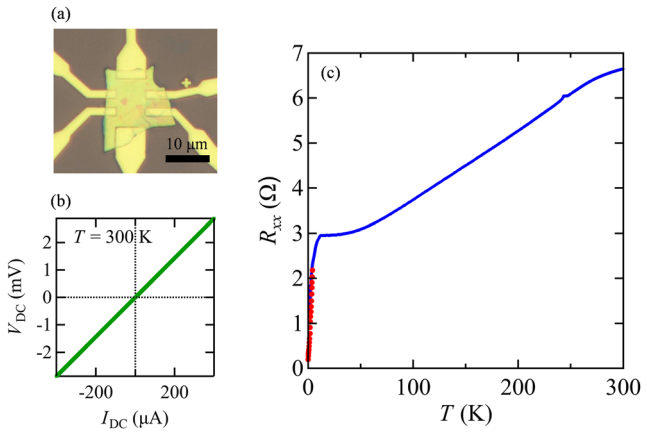

FIG. 3. (a) Optical micrograph of exfoliated ReN_2 with Au/Cr metal electrodes on a SiO_2/Si substrate (sample no. 1). (b) Current–voltage characteristic at T = 300 K. (c) Temperature dependence of longitudinal resistance measured at 1.5–300 K in a variable temperature insert (blue) and at 0.06–2.5 K in a dilution refrigerator (red).

Figure 3(b) shows the I-V curve of sample no. 1 at T = 300 K. The curve displays linearity, and R_{xx} obtained from the slope is as small as 4.2 Ω. The derived volume resistivity (ρ_V) and sheet resistivity (ρ_S) are $\rho_V = 9.8 \times 10^{-8}$ Ωm and $\rho_S = 1.63$ Ω, respectively. As shown in Fig. 3(c), R_{xx} decreases as the temperature decreases. The sheet carrier density at T = 300 K for a ReN_2 bilayer unit was derived as $n = 4.1 \times 10^{14}$ cm^{-2} from measured Hall resistance R_{xy}. All these transport properties show characteristic features of metallic materials. Therefore, we can derive the simple but very important fundamental conclusion that ReN_2 is a metal. Similar results were observed for sample no. 2 (Fig. S1), which confirms this conclusion.

Furthermore, the temperature dependence of R_{xx} revealed another feature of ReN_2 —superconductivity. R_{xx} drops rapidly at approximately T = 10 K to 1.3 Ω at T = 1.5 K [the blue line in Fig. 3(c)]. For the measurements at temperatures below 1.5 K, we moved the sample from the VTI to the dilution refrigerator. As the temperature decreases, R_{xx} decreases down to vanishingly small resistance 0.18 Ω at T = 60 mK [the red dots in Fig. 3(c)].

When an external magnetic field H is applied to the ReN_2, R_{xx} increases and saturates as shown in Figs. 4(a) and 4(b). This confirms the superconductivity. Suppression of R_{xx} breaks down more significantly in the perpendicular magnetic field $H_\perp$ than in the parallel magnetic field $H_{//}$. We define the critical temperature of superconductivity as the onset temperature $T_{c,onset}$ such that R_{xx} drops by 5% of R_{xx} at T = 12 K; H vs $T_{c,onset}$ is plotted in Fig. 4(c). The linear extrapolations of $H_{//}$ and $H_\perp$ give 98.19 T and 8.89 T at $T_{c,onset}$ = 0, respectively. To derive the upper critical fields at zero temperature, we adopted Werthamer-Helfand-Hohenberg (WHH) theory, which provides the estimate of upper critical field of type-II superconductors[20]

$$H_{c2}(0) = -0.693 T_c (dH_{c2}/dT)_{Tc}. \quad (1)$$

The upper critical fields for parallel and perpendicular magnetic fields at zero temperature are derived as $H_{c2,//}(0)$ = 68 T and $H_{c2,\perp}(0)$ = 6.16 T from the linear extrapolations of the experimental data. The anisotropic ratio was estimated as $H_{c2,//}(0)/H_{c2,\perp}(0) \cong 11$. Assuming the zero-field critical temperature $T_{c0} \sim 10$ K from Fig. 4(b), the Pauli paramagnetic limit H_P is estimated as $H_P \approx 1.84\, T_{c0}$ = 18.4 T.[20,21] The upper critical field obtained using the WHH theory ($H_{c2,//}(0)$ = 68 T) far exceeds its Pauli limit by a factor of ~4. Although the origin of this enhancement in ReN_2 is controvertible, in the case of $NbSe_2$, H_P is larger than $H_{c2,//}(0)$ by a factor of ~6.5 for monolayer and is understood based on spin-orbit interactions.[22]

To further characterize the superconducting anisotropy in ReN_2 quantitatively, we conducted R_{xx} measurements with different angles θ of applied magnetic fields H at T = 100 mK. Figure 5(a) shows the R_{xx} vs H plot for θ ranging from 90° (perpendicular) to 0° (in plane). To evaluate the anisotropy, we defined the critical magnetic field of superconductivity as $H_{c(1.5\,\Omega)}$, where R_{xx} exceeds 1.5 Ω and plotted $H_{c(1.5\Omega)}$ as a function of θ [Fig. 5(b)]. The anisotropic ratio was calculated as $H_{c(1.5\,\Omega)}$ (θ = 0°)/$H_{c(1.5\Omega)}$ (θ = 90°) ≅ 33.2. We show color-scale plots of dV/dI as a function of I_{DC} and H with I_{AC} = 2.5 μA [Fig. 5(c)]. The dip of dV/dI is suppressed as H increases, and the dip is more effectively suppressed as θ approaches 90°. The same tendency is observed in sample no. 2 (Fig. S1d). The different behavior in the direction of

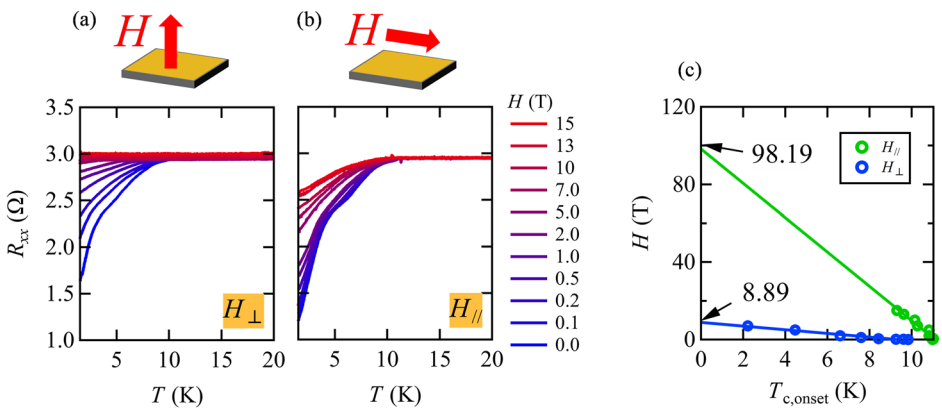

FIG. 4. Temperature dependence of R_{xx} in (a) a parallel magnetic field $H_{//}$ and (b) a perpendicular magnetic field $H_\perp$. (c) Plot of H vs $T_{c,onset}$. The green and blue lines show linear fit to the data for $H_{//}$ and $H_\perp$, respectively.

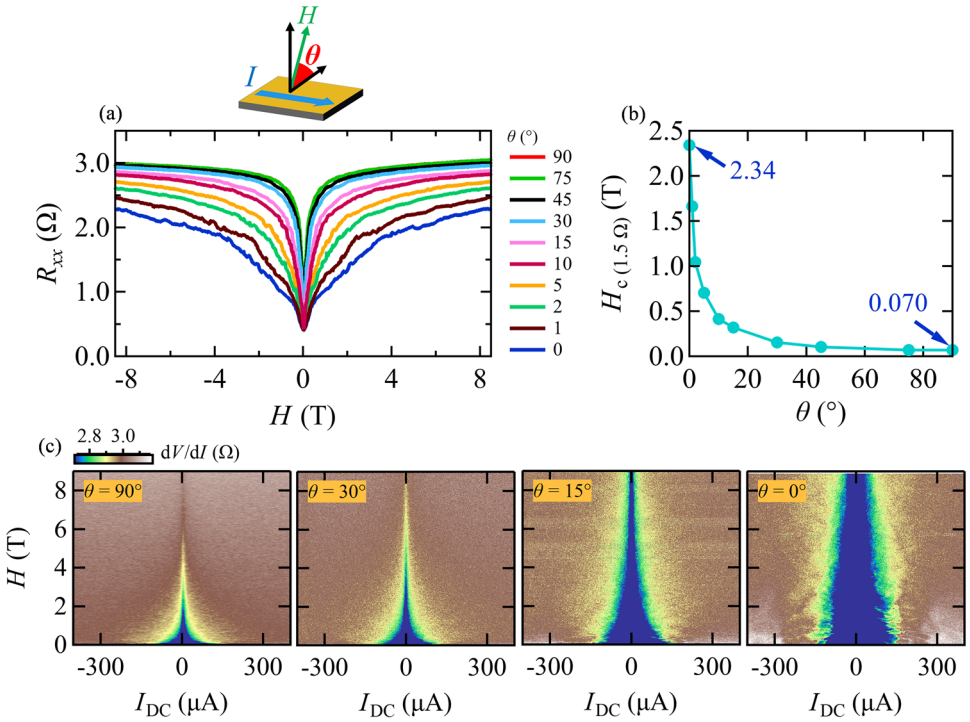

FIG. 5. (a) Magnetic field dependence of R_{xx} in different applied magnetic field angles θ. (b) Plot of critical magnetic field, where R_{xx} exceeds 1.5 Ω, as a function of θ. (c) Color maps of dV/dI as a function of I_{DC} and H with different θ at T = 100 mK.

applied magnetic fields indicates that ReN_2 is an anisotropic layered superconductor.

Here, we should note that the superconductivity of the exfoliated ReN_2 flakes observed in the present work is distinguished from superconductivity of pure Re in two ways: the critical temperature and critical magnetic field of superconductivity in Re are $T_c \sim 1.7$ K[23] and $H_c \sim 0.02$ T,[24] respectively, both of which are smaller than those of ReN_2. Therefore, the observed superconductivity is inherent to ReN_2.

The distinguishing feature of 2D superconducting materials is that they can be combined with other 2D materials, leading to interesting physical phenomena. For example, utilizing $NbSe_2$, which is one of the most commonly used layered superconductors that exhibit superconductivity even after exfoliated down to one atomic layer,[22] the Josephson effect and the Andreev reflection were observed from $NbSe_2/NbSe_2$[25] and graphene/$NbSe_2$[26] van der Waals junctions, respectively. However, $NbSe_2$ is easily oxidized in the air. The oxide layer formed on the surface increases the junction resistance at the van der Waals interfaces and the contact resistance at the junctions to the metal electrodes. To prevent this oxidization, one should treat the material in a glove box and/or avoid heating during the resist-baking procedure in lithography processes. In contrast, STEM and EDX of ReN_2 near the surface (Fig. S2) indicates that there is no oxidized layer on the surface. In addition, contact resistance at the junction between the exfoliated ReN_2 surface and the metal electrodes is small ($R_{contact} < 20\ \Omega$), even though we exfoliated ReN_2 crystals in the atmosphere and heated it at 170 °C for 20 min during the resist-baking procedure. Thus, the stability of ReN_2 can be a key advantage for incorporation into van der Waals heterostructures.

Finally, to provide microscopic insight into the electronic and optical properties of ReN_2, we carried out first principles calculations based on density functional theory,[27,28] implemented using the Quantum ESPRESSO (opEn-Source Package for Research in Electronic Structure, Simulation, and Optimization) package.[29] For the exchange–correlation energy among electrons and electron–ion interaction, we use GGA-PBE[30] and projector augmented wave pseudopotentials,[31] respectively. The valence wave functions and augmented charge density were expanded by a plane wave basis set with cutoff energies of 70 Ry and 560 Ry, respectively. The Brillouin-zone integration was performed under a 45 × 45 × 15 uniform k-point grid.[32] The geometric structure of ReN_2 bulk crystal was optimized under the experimental lattice constants ($a = b = 2.806$ Å, $c = 10.747$ Å)[5] until the remaining force acting on the atoms was less than 0.0001 Ry/Bohr. Figure 6(a) shows the electronic structure of ReN_2. Four dispersive bands cross the Fermi level indicate that the ReN_2 is a metal. Indeed, it has a substantial density of states (DOS) at the Fermi level [Fig. 6(b)]. To provide theoretical insight into the red translucency of ReN_2, we investigated absorption spectra under the polarization normal and parallel to the ReN_2 layer [Fig. 6(c)]. The optical absorption spectra were estimated from the real and imaginary parts of the dielectric function based on the independent-particle approximation model using the epsilon.x code in the Quantum ESPRESSO package. For both parallel and normal polarization, absorption is absent around the energy of 1.8 eV, while there is substantial absorption for the rest of the energy ranges leading to the unusual translucent properties and the transmittance of red light. These results are roughly consistent with the calculation with the GGA and HSE (Heyd–Scuseria–Ernzerhof) functionals.[33]

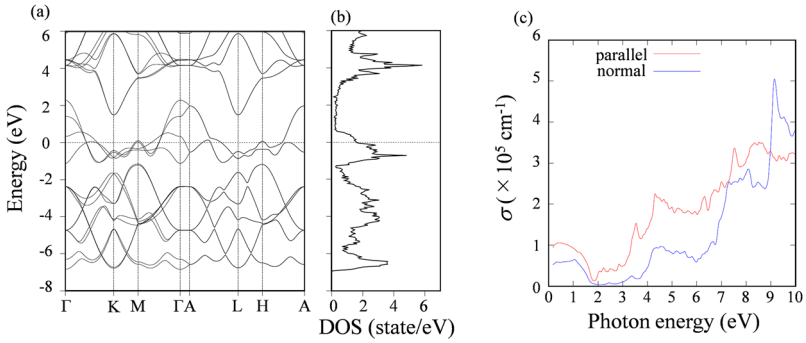

FIG. 6. (a) Electronic band structure and (b) density of states in a ReN_2 bulk crystal. Energy is measured from that of the Fermi level. (c) Calculated absorption spectra of a ReN_2 bulk crystal with light polarization parallel and normal to the ReN_2 layer. The red and blue curves correspond to the absorption parallel and normal to the layer, respectively.

In conclusion, we presented the electrical transport study of ReN_2 for the first time after the synthesis of the ReN_2 crystal. We confirmed that ReN_2 is a metal, which is supported both by transport measurements and band calculations. ReN_2 also exhibits a signature of superconductivity, which is anisotropic in the direction of applied magnetic fields. We should note that there is room for development in the quality of the ReN_2 crystal. We suppose that the broad superconductivity transition with a stepwise decrease in R_{xx}, the finite residual resistance at 60 mK observed in the temperature dependence of R_{xx}, and the variation in T_c between samples might be attributed to the inhomogeneity in the ReN_2 flake. At the moment, the dependence of T_c on the thickness of ReN_2 flakes is not clear. Nevertheless, ReN_2 provides a new option for a 2D superconductor, which can be utilized without concern for oxidization.

See supplementary material for Figs. S1 and S2.

This work was supported by CREST, Japan Science and Technology Agency (JST), under Grant No. JPMJCR15F3 and by JSPS KAKENHI under Grant Nos. JP19H02542 and JP19H01820.

REFERENCES

[1] H. Sumiya and S. Satoh, Diamond Relat. Mater. **5**, 1359 (1996).
[2] H. Sumiya, K. Harano, and K. Tamasaku, Diamond Relat. Mater. **58**, 221 (2015).
[3] T. Taniguchi and S. Yamaoka, J. Cryst. Growth **222**, 549 (2001).
[4] T. Taniguchi and K. Watanabe, J. Cryst. Growth **303**, 525 (2007).
[5] F. Kawamura, H. Yusa, and T. Taniguchi, Appl. Phys. Lett. **100**, 251910 (2012).
[6] B. Jariwala, D. Voiry, A. Jindal, B. A. Chalke, R. Bapat, A. Thamizhavel, M. Chhowalla, M. Deshmukh, and A. Bhattacharya, Chem. Mater. **28**, 3352 (2016).
[7] K. Keyshar, Y. Gong, G. Ye, G. Brunetto, W. Zhou, D. P. Cole, K. Hackenberg, Y. He, L. Machado, M. Kabbani, A. H. C. Hart, B. Li, D. S. Galvao, A. George, R. Vajtai, C. S. Tiwary, and P. M. Ajayan, Adv. Mater. **27**, 4640 (2015).
[8] M. Hafeez, L. Gan, H. Li, Y. Ma, and T. Zhai, Adv. Mater. **28**, 8296 (2016).
[9] M. Hafeez, L. Gan, A. Saleem Bhatti, and T. Zhai, Mater. Chem. Front. **1**, 1917 (2017).
[10] S. Yang, C. Wang, H. Sahin, H. Chen, Y. Li, S.-S. Li, A. Suslu, F. M. Peeters, Q. Liu, J. Li, and S. Tongay, Nano Lett. **15**, 1660 (2015).
[11] D. Wolverson, S. Crampin, A. S. Kazemi, A. Ilie, and S. J. Bending, ACS Nano **8**, 11154 (2014).
[12] D. A. Chenet, O. B. Aslan, P. Y. Huang, C. Fan, A. M. van der Zande, T. F. Heinz, and J. C. Hone, Nano Lett. **15**, 5667 (2015).
[13] Y.-C. Lin, H.-P. Komsa, C.-H. Yeh, T. Björkman, Z.-Y. Liang, C.-H. Ho, Y.-S. Huang, P.-W. Chiu, A. V. Krasheninnikov, and K. Suenaga, ACS Nano **9**, 11249 (2015).
[14] C. M. Corbet, C. McClellan, A. Rai, S. S. Sonde, E. Tutuc, and S. K. Banerjee, ACS Nano **9**, 363 (2015).
[15] E. Zhang, P. Wang, Z. Li, H. Wang, C. Song, C. Huang, Z.-G. Chen, L. Yang, K. Zhang, S. Lu, W. Wang, S. Liu, H. Fang, X. Zhou, H. Yan, J. Zou, X. Wan, P. Zhou, W. Hu, and F. Xiu, ACS Nano **10**, 8067 (2016).
[16] S. Yang, S. Tongay, Q. Yue, Y. Li, B. Li, and F. Lu, Sci. Rep. **4**, 5442 (2015).
[17] S. Wang, H. Ge, S. Sun, J. Zhang, F. Liu, X. Wen, X. Yu, L. Wang, Y. Zhang, H. Xu, J. C. Neuefeind, Z. Qin, C. Chen, C. Jin, Y. Li, D. He, and Y. Zhao, J. Am. Chem. Soc. **137**, 4815 (2015).
[18] F. Wu, C. Huang, H. Wu, C. Lee, K. Deng, E. Kan, and P. Jena, Nano Lett. **15**, 8277 (2015).
[19] Z. Liu, J. Liu, and J. Zhao, Nano Res. **10**, 1972 (2017).
[20] N. R. Werthamer, E. Helfand, and P. C. Hohenberg, Phys. Rev. **147**, 295 (1966).
[21] B. S. Chandrasekhar, Appl. Phys. Lett. **1**, 7 (1962).
[22] X. Xi, Z. Wang, W. Zhao, J.-H. Park, K. T. Law, H. Berger, L. Forró, J. Shan, and K. F. Mak, Nat. Phys. **12**, 139 (2016).
[23] A. U. Haq and O. Meyer, Thin Solid Films **94**, 119 (1982).
[24] J. K. Hulm and B. B. Goodman, Phys. Rev. **106**, 659 (1957).
[25] N. Yabuki, R. Moriya, M. Arai, Y. Sata, S. Morikawa, S. Masubuchi, and T. Machida, Nat. Commun. **7**, 10616 (2016).
[26] D. K. Efetov, L. Wang, C. Handschin, K. B. Efetov, J. Shuang, R. Cava, T. Taniguchi, K. Watanabe, J. Hone, C. R. Dean, and P. Kim, Nat. Phys. **12**, 328 (2016).
[27] P. Hohenberg and W. Kohn, Phys. Rev. **136**, B864 (1964).
[28] W. Kohn and L. J. Sham, Phys. Rev. **140**, A1133 (1965).
[29] P. Giannozzi, S. Baroni, N. Bonini, M. Calandra, R. Car, C. Cavazzoni, D. Ceresoli, G. L. Chiarotti, M. Cococcioni, I. Dabo, A. Dal Corso, S. de Gironcoli, S. Fabris, G. Fratesi, R. Gebauer, U. Gerstmann, C. Gougoussis, A. Kokalj, M. Lazzeri, L. Martin-Samos, N. Marzari, F. Mauri, R. Mazzarello, S. Paolini, A. Pasquarello, L. Paulatto, C. Sbraccia, S. Scandolo, G. Sclauzero, A. P. Seitsonen, A. Smogunov, P. Umari, and R. M. Wentzcovitch, J. Phys.: Condens. Matter **21**, 395502 (2009).
[30] J. P. Perdew, K. Burke, and M. Ernzerhof, Phys. Rev. Lett. **77**, 3865 (1996).
[31] A. Dal Corso, Comput. Mater. Sci. **95**, 337 (2014).
[32] H. J. Monkhorst and J. D. Pack, Phys. Rev. B **13**, 5188 (1976).
[33] S.-H. Zhang and B.-G. Liu, "Two-dimensional ReN_2 materials from first principles," e-print arXiv:1612.02748 (2016).